Numerical Simulations of an Oblique Detonation Wave Engine

Jean-Luc Cambier*
ANALATOM Inc., San Jose, California
and
Henry Adelman† and Gene P. Menees‡
NASA Ames Research Center, Moffett Field, California

A code for the simulations of supersonic combustion has been developed and applied to flow computations relevant to the concept of the oblique detonation wave engine (ODWE). In a previous paper, it was shown that a stable oblique detonation wave, attached to a ramp, could be obtained in a homogeneous fuel-air mixture. In the following, the total variation diminishing (TVD) code is used to simulate the effect of mixing fluctuations on the detonation front. An arbitrary, periodic variation of the equivalence ratio is modeled first and then compared with the wave obtained at similar conditions for a uniformly mixed flow. It is seen that original fluctuations in front curvature, due to Mach number variations, are amplified by the combustion, but the overall influence of the heat release is somewhat lessened. A more severe flow condition is then simulated by injecting fuel through two struts; in this worst mixing scenario, the curvature in the wave front is dominated by the mixing fluctuations, with little influence from combustion. The shock still acts as a flame holder; this indicates that although the oblique detonation front is replaced by a more complicated structure, the concept of ODWE can be generalized to realistic configurations.

Nomenclature

C_p = specific heat at constant pressure
C_v = specific heat at constant volume
c = (frozen) speed of sound
$\hat{c}_s$ = mass fraction specie s, $(=\rho_s/\rho)$
D_t = turbulent diffusion coefficient
dS = surface element
dV = cell volume
E = total energy density
H = total enthalpy density
h_s^o = formation enthalpy of specie s
$\mathfrak{L}_s$ = chemical removal rate
M_s = molecular weight of specie s
$\boldsymbol{m}$ = momentum density, $(=\rho u, \rho v)$
P = total pressure
$\mathcal{P}_s$ = chemical production rate
Pr_t = turbulent Prandtl number
$\boldsymbol{q}$ = heat flux
$\hat{R}$ = universal gas constant
Sc_t = turbulent Schmidt number
u = x-component of velocity field
V_D = diffusion velocity
v = y-component of velocity field
X_s = molar concentration of specie s
$\alpha^{(k)}$ = generalized Riemann invariant
γ = ratio of specific heats
η = dynamic viscosity
κ = heat conductivity
ξ = unit vector normal to interface
ρ = mixture mass density
ρ_s = mass density of specie s
σ = viscous stress tensor
Φ = dissipation flux

Received April 8, 1988; revision received Nov. 8, 1988.

*Research Scientist.
†Research Scientist, Aerothermodynamics Branch. Member AIAA.
‡Research Scientist, Aerothermodynamics Branch. Associate Member AIAA.

I. Introduction

THE use of detonations as ignition mechanisms in scramjet designs goes as far back as 1946.[1] Subsequent work on the subject finally led to the use of oblique detonation waves as the most effective design of detonative ramjets.[2,4] However, the experimental evidence for stable, oblique detonation waves (ODW) is sketchy.[5-10] To remedy this situation, an experiment is being designed to verify the existence of a standing detonation on a wedge and prove the validity of the ODW engine concept.[11] There is also a need for accurate numerical simulations of the reacting flowfield, both the design purposes and for analysis. To this effect, a new code is being developed, based on an explicit, second-order total variation diminishing (TVD) scheme.[12-17] Viscous, diffusive, and chemical processes are added to the scheme by an operator-splitting method. The overall scheme is second-order accurate in space and first-order accurate in time. (Individual processes, such as convection and chemical kinetics, are second-order accurate in time, but the coupling reduces the overall time accuracy to the first order.) The code has a multigridding capability, where grids are patched along their common boundaries. The patching process is exactly flux conservative.

The code has been applied to the numerical simulations of a generic strut configuration, where fuel (H_2) is injected and mixed with air. Downstream of the injector is a wedge that will support a detonation wave. The overall flowfield occupies several grids. The downstream boundary conditions at each

station are taken as upstream boundary conditions for the next grid, to insure continuity. We first discuss the methods used, then we present some numerical results obtained. The numerical results presented here are only a first attempt at modeling the features of supersonic mixing and combustion; the numerical capability needs further development and validation.

II. Numerical Method

We are solving the two-dimensional Navier-Stokes equations for multiple species:

$$\frac{\partial Q}{\partial t}+\frac{\partial F}{\partial x}+\frac{\partial G}{\partial y}+\frac{\partial F_v}{\partial x}+\frac{\partial G_v}{\partial y}=S \tag{1}$$

where the right-hand side represents the viscous fluxes, diffusive fluxes, and chemical source terms to be described later. The variables and inviscid fluxes are

$$Q=\begin{pmatrix}\rho_1\\ \vdots\\ \rho_N\\ \rho u\\ \rho v\\ E\end{pmatrix}\qquad F=\begin{pmatrix}\rho_1 u\\ \vdots\\ \rho_N u\\ P+\rho u^2\\ \rho uv\\ u(P+E)\end{pmatrix}\qquad G=\begin{pmatrix}\rho_1 v\\ \vdots\\ \rho_N v\\ \rho uv\\ P+\rho v^2\\ v(P+E)\end{pmatrix}$$

The total energy is

$$E=\rho\int C_v dT+\tfrac{1}{2}\rho(u^2+v^2)+\Sigma_s\rho_s h_s^o \tag{2}$$

and the pressure is obtained by Dalton's law:

$$\mathrm{P}=\sum_s \rho_s\frac{\hat{R}}{M_s}T \tag{3}$$

The (frozen) speed of sound is obtained from

$$c^2=\left(\sum_s \hat{c}_s\frac{\partial P}{\partial \rho_s}\right)_{m,E}+\left[(H-u^2-v^2)\frac{\partial P}{\partial E}\right]_{\rho,m} \tag{4}$$

and the ρ_s are linearly independent. The nonlinear hyperbolic system [Eq. (1)] can be transformed into the characteristic equation by means of a transformation matrix T and its inverse. We partition the volume into quadrilateral cells and denote them by a pair of indices (i,j). (Thereafter, the second index will be omitted, when possible.) The interface between two cells is then denoted by $(i+\tfrac{1}{2},j)$ and $(i,j+\tfrac{1}{2})$. If $\lambda_{i+\frac{1}{2}}^{(k)}$ is the spectrum of eigenvalues and $w_i^{(k)}$ the characteristic variables, the hyperbolic system composed of the Euler equations becomes the system of uncoupled characteristic equations:

$$\frac{\partial w_i^{(k)}}{\partial t}+\lambda_i^{(k)}\frac{\partial w_i^{(k)}}{\partial x}=0 \tag{5}$$

The transformation matrix T is composed of the left eigenvectors. Any discontinuity breaks up into characteristic waves, each carrying the generalized Riemann invariants $\alpha_{i+\frac{1}{2}}^{(k)}=w_{i+1}^{(k)}-w_i^{(k)}$. The original and characteristic variables are related by

$$\Delta_{i+\frac{1}{2}}Q=T_{i+\frac{1}{2}}\alpha_{i+\frac{1}{2}}$$

$$\Delta_{i+\frac{1}{2}}F=T_{i+\frac{1}{2}}\Lambda_{i+\frac{1}{2}}\alpha_{i+\frac{1}{2}}$$

To solve the Euler system numerically, we use a finite volume algorithm. The scheme is, therefore, written in a conservative form:

$$Q^{n+1}=Q^n+\frac{\Delta t}{\Delta V}\left[\sum F dS\right] \tag{6}$$

The interface between two cells defines a surface element dS, and its orientation is obtained by the unit vector normal to the interface $\xi=dS/|dS|$.

The fluxes F are composed of an interface-centered flux $\langle F\rangle$ and a diffusive part:

$$F_{i+\frac{1}{2}}=\langle F_{i,i+1}\rangle+T_{i+\frac{1}{2}}\Phi_{i+\frac{1}{2}} \tag{7}$$

where $\langle\ \rangle$ denote an arithmetic average. The diffusive flux Φ is obtained after transformation to the characteristic variables. The spectrum of eigenvalues is

$$\{\lambda^{(k)}\}=\{u_n,\ \ldots,\ u_n,\ u_n+c,\ u_n-c\}$$

$$u_n=\xi_x u+\xi_y v$$

i.e., u_n is the component of the velocity normal to the cell interface. The averaging method to define the eigenvectors and eigenvalues at the interface could be chosen to be the arithmetic average $\langle\ \rangle$ or Roe's method.[18] The latter method is strictly valid for ideal gases. However, it can be used as an excellent approximation for real gases.

The diffusion flux is given by

$$\Phi_{i+\frac{1}{2}}=\tfrac{1}{2}\left(g_i+g_{i+1}-|\lambda^*_{i+\frac{1}{2}}|\alpha_{i+\frac{1}{2}}\right) \tag{8}$$

where

$$\lambda^*_{i+\frac{1}{2}}=\begin{cases}\lambda_{i+\frac{1}{2}} & \text{if } \lambda_{i+\frac{1}{2}}\Delta t/\Delta x>\epsilon\\ \epsilon\Delta x/\Delta t & \text{otherwise}\end{cases}$$

A small ($\simeq 0.1$) entropy-violating parameter ϵ plays the role of an artificial viscosity and is necessary to prevent rarefaction shocks. This parameter also induces an artificial shear at a slipstream, which becomes negligible compared to the true shear-stress modeled after the Navier-Stokes equations if the grid spacing is made small enough. Note that the time step Δt used above should be the time scale of convection. If the actual time step is forced to small values by some other process (viscosity, chemical kinetics), then the actual Courant number is forced to small values: $\lambda\Delta t/\Delta x<\epsilon$. Applying the cutoff described above may yield a flux Φ that is overly diffusive. This effect was originally noticed in one-dimensional computations of unsteady detonations; therefore, the Δt to be used should be the convection time scale only. The flux limiter g_i is obtained by the following steps:

$$\tilde{g}_{i+\frac{1}{2}}^{(k)}=\frac{1}{2}\left[\lambda_{i+\frac{1}{2}}^{*(k)}-\frac{\Delta x}{\Delta t}(\mu_{i+\frac{1}{2}}^{(k)})^2\right]\alpha_{i+\frac{1}{2}}^{(k)} \tag{9}$$

$$g_i^{(k)}=s_{i+\frac{1}{2}}^{(k)}\max\left[0,\min\left(|\tilde{g}_{i+\frac{1}{2}}^{(k)}|,\tilde{g}_{i-\frac{1}{2}}^{(k)}s_{i+\frac{1}{2}}^{(k)}\right)\right] \tag{10}$$

with

$$s_{i+\frac{1}{2}}^{(k)}=\mathrm{sign}(\tilde{g}_{i+\frac{1}{2}}^{(k)})$$

$$\mu_{i+\frac{1}{2}}^{(k)}=\lambda_{i+\frac{1}{2}}^{(k)}\Delta t/\Delta x$$

Observe that without the flux-limiter g_i, the diffusive flux in Eq. (8) reduces the overall scheme to the first-order upwind method. More compressive forms of the flux-limiter than Eq. (10) have been published (see Ref. 14 for a review) and some have been experimented with by the present authors. We found no significant cost variations between our present upwind scheme and the symmetric scheme of Yee et al.[14] The best resolution of the discontinuities (especially contact discontinuities) is obtained with a generalization of the so-called "superbee" limiter:

$$g_i^{(k)}=s_{i+\frac{1}{2}}^{(k)}\max\left[0,\min\left(\nu|\tilde{g}_{i+\frac{1}{2}}^{(k)}|,\tilde{g}_{i-\frac{1}{2}}^{(k)}s_{i+\frac{1}{2}}^{(k)}\right),\right.$$
$$\left.\min\left(|\tilde{g}_{i+\frac{1}{2}}^{(k)}|,\nu\tilde{g}_{i-\frac{1}{2}}^{(k)}s_{i+\frac{1}{2}}^{(k)}\right)\right] \tag{11}$$

where $\nu=2$ for one-dimensional problems. For two-dimensional problems (with a dimensional splitting), this choice is too compressive, and we found that $\nu\simeq 1.5$ gives the best results. However, the continuity at grid boundaries is not as well reproduced. To keep a smooth behavior at the grid boundaries, when multiple grids are used, we need to limit ourselves to $\nu=1$, i.e., the limiter (10). Another alternative was to make the parameter of artificial compression ν a local quantity; the results showed sharper discontinuities, although the method became somewhat cumbersome. We therefore concluded that the choice of flux limiters gives small improvements that are not of considerable significance unless one can safely use a very compressive limiter such as Eq. (11), with $\nu=2$. This latter choice would be possible if there were enough grid adaptation, such that the cell interfaces are nearly aligned with the discontinuities. No grid-adapting method has yet been included in the present version of the code.

The jumps in characteristic variables are for a case with N_s species:

$$\alpha^s_{i+\frac{1}{2},j} = \Delta\rho_s - \hat{c}_s \Delta P/c^2 \tag{12}$$

$$\alpha^{N_s+1}_{i+\frac{1}{2},j} = \xi_y(\Delta m_x - u_{i+\frac{1}{2},j}\Delta\rho) - \xi_x(\Delta m_y - v_{i+\frac{1}{2},j}\Delta\rho) \tag{13}$$

$$\alpha^{N_s+2}_{i+\frac{1}{2},j} = \frac{1}{2c^2}(\Delta P + c\Delta m_n - cu_n\Delta\rho) \tag{14}$$

$$\alpha^{N_s+3}_{i+\frac{1}{2},j} = \frac{1}{2c^2}(\Delta P - c\Delta m_n + cu_n\Delta\rho) \tag{15}$$

where $m_n=\xi_x m_x+\xi_y m_y$, and $\hat{c}_s=\rho_s/\rho$. Note that, strictly speaking, the jump in pressure ΔP should be evaluated in functions of the changes of the original variables, i.e.,

$$\tilde{\Delta}P = \sum_s \frac{\partial P}{\partial \rho_s}\Delta\rho_s + \frac{\partial P}{\partial m_x}\Delta m_x + \frac{\partial P}{\partial m_y}\Delta m_y + \frac{\partial P}{\partial E}\Delta E \tag{16}$$

This expression is nothing but the differential of the pressure on our discrete lattice. Replacing this expression by $\Delta P=P_{i+1}-P_i$ leads to slightly less diffusive results at a slightly lesser cost.

The method described above applies for problems with a one-dimensional structure. To generalize to two (or more) dimensions, one splits the operator into unidirectional sweeps, in the ξ (or i) and η (or j) directions. The complete operation takes the following form:

$$\delta_\xi Q = \frac{\Delta t}{\Delta V}\left[\boldsymbol{F}_{i-\frac{1}{2},j}d\boldsymbol{S}_{i-\frac{1}{2},j} + \boldsymbol{F}_{i+\frac{1}{2},j}d\boldsymbol{S}_{i+\frac{1}{2},j}\right]$$

$$\delta_\eta Q = \frac{\Delta t}{\Delta V}\left[\boldsymbol{F}_{i,j-\frac{1}{2}}d\boldsymbol{S}_{i,j-\frac{1}{2}} + \boldsymbol{F}_{i,j+\frac{1}{2}}d\boldsymbol{S}_{i,j+\frac{1}{2}}\right]$$

$$Q^{n+1} = Q^n + \delta_\xi Q^n + \delta_\eta Q^n \tag{17}$$

III. Viscous and Diffusive Terms

The viscous fluxes are

$$F_v = \begin{pmatrix} j_x^1 \\ \vdots \\ j_x^N \\ -\sigma_{xx} \\ -\sigma_{xy} \\ q_x \end{pmatrix} \qquad G_v = \begin{pmatrix} j_y^1 \\ \vdots \\ j_y^N \\ -\sigma_{xy} \\ -\sigma_{yy} \\ q_y \end{pmatrix}$$

where $\boldsymbol{j}$ is the diffusion flux of the chemical species, $\bar{\bar{\sigma}}$ is the stress tensor, and $\boldsymbol{q}$ is the heat flux. By definition

$$\sigma_{xx} = \eta\left(\frac{4}{3}\frac{\partial u}{\partial x} - \frac{2}{3}\frac{\partial v}{\partial y}\right) \tag{18}$$

$$\sigma_{yy} = \eta\left(\frac{4}{3}\frac{\partial v}{\partial y} - \frac{2}{3}\frac{\partial u}{\partial x}\right) \tag{19}$$

$$\sigma_{xy} = \eta\left(\frac{\partial u}{\partial y} + \frac{\partial v}{\partial x}\right) \tag{20}$$

and the heat flux is given by

$$\boldsymbol{q} = -\kappa\nabla T - \bar{\bar{\sigma}}\boldsymbol{u} + \sum_s \boldsymbol{j}^s h_s \tag{21}$$

We have neglected the Dufour term, i.e., the term involving the thermal diffusion coefficient in the expression of the heat flux. We have written algorithms for the computation of the laminar, multicomponent diffusion terms, although they are not included in the following numerical simulations. Given the wide range of temperatures accessible in combusting flows, we have found that a unique power-law model of the transport coefficients is too sensitive to be accurate over the whole temperature range. Therefore, the laminar transport coefficients were estimated using the Lennard-Jones model of intermolecular interactions: tables of the collison integral $\Omega^{*(l,s)}_{rs}$ can be found in Refs. 19 and 20. See Dixon-Lewis[19] for detailed expressions of the transport coefficients, including the binary and multicomponent diffusion coefficients. The solution of the laminar diffusive fluxes is obtained form an algorithm by Boris and Jones,[21] also discussed in Ref. 19.

In the situations we are studying, the turbulent processes are found to be the dominant diffusion mechanisms; therefore, the laminar diffusive fluxes need not to be computed. Instead, the turbulent diffusion alone is computed and is modeled by a Fickian process:

$$\boldsymbol{j}_s \simeq -\rho D_t \nabla \hat{c}_s \tag{22}$$

The computational work is considerably reduced, but the modeling is less accurate. Since turbulent transport is a molar rather than a molecular phenomenon, there is no accurate modeling from kinetic theory. If $[\eta_t]$ is the turbulent viscosity, we obtain the other parameters by

$$\kappa_t = C_p\eta_t/Pr_t$$

$$\rho D_t = \eta_t/Sc_t$$

The turbulent Prandtl and Schmidt numbers are assumed to be both equal to 0.9. The turbulent viscosity is estimated from the mixing-length model, with the Smagorinski[22] length scale (see also Ref. 23)

$$\eta_t = \rho\tfrac{1}{2}(C\Delta)^2|S_{xy}| \tag{23}$$

with $C\simeq 0.19$ a constant

$$|S_{xy}| = \left[\left(\frac{\partial u}{\partial y}\right)^2 + \left(\frac{\partial v}{\partial x}\right)^2\right]^{\frac{1}{2}} \tag{24}$$

is the strain-rate and Δ is the scale of the smallest resolved eddies, determined by the grid size: $\Delta\simeq\max(\Delta x,\Delta y)$. This model is expected to be valid in the wake region.

Near the wall, the turbulent mixing-length scale is assumed to follow the law

$$\Delta \simeq \kappa_{v_K} y\left[1 - e^{-y^+/A^+}\right] \tag{25}$$

where $\kappa_{v_K}\simeq 0.4$ is the von Kármán constant, y is the distance normal to the wall, and the dimensionless variable

$$y^+ = \rho\frac{U_w y}{\eta_l} \tag{26}$$

is scaled by the constant $A^+ = 26$. In our numerical simulations, the grid is clustered near the body walls, but such that the spacing does not change by more than 5% between adjacent cells in order to conserve second-order accuracy.[24] This turbulence model is admittedly very crude. It is currently being improved and will accommodate other effects, such as the transition to turbulence, intermittency, and blowing effects.

IV. Chemical Kinetics

When coupling the chemistry to the fluid dynamics by the operator-splitting method, one assumes that the time step is too short for convective (or diffusive) processes to be important. As the temperature of the mixture increases by an amount ΔT during a time τ_{chem} due to combustion, the inertia of the gas is such that the effect on neighboring cells is not felt before a characteristic time $\tau_{\text{conv}} \simeq \Delta x/|u|+c$. The global time step can therefore be an intermediate between the two fundamental time scales. At the end of the chemical step, the temperature is obtained by solving iteratively the equation $e_{\text{int}} \simeq E - \frac{1}{2}\rho(u^2+v^2) \simeq \rho\int C_v(T)dT$, where e_{int}, the internal energy (which includes the energies of formation), is assumed constant during the step. In average, only a few iterations (≤ 5) are necessary for convergence.

Let us denote the production and losses rates by $\mathcal{P}_s, \mathcal{L}_s$, such that

$$\frac{dn_s}{dt} = \mathcal{P}_s - \mathcal{L}_s n_s = \dot{w}_s n_s \tag{27}$$

where $\mathcal{P}_s, \mathcal{L}_s$ are evaluated from the Arrhenius rates and other species concentrations at a given time level. The combustion proceeds via 1) an induction period τ_i, during which radical species (chain-branching) buildup, 2) a heat-release period τ_r, and 3) an equilibriation period τ_{eq}. The time step δt used in the integration of Eq. (27) is estimated at each time level by the rates of change $\dot{w}_s$ of "relevant" species, i.e., those with a significant concentration, such that a maximum relative change of $\simeq 10\%$ is allowed. The smallest time steps are found during the heat release period. To integrate to the next time level $t_{\text{chm}} + \delta t$, we will use a predictor-corrector method to evaluate the rates and concentrations at time level $t_{\text{chm}} + \frac{1}{2}\delta t$, for time centering. If the predictor-corrector fails to produce convergence after a few iterations, the time step is reduced and the procedure is repeated.

Since the chemical time step δt may be different in each cell, we need a time counter t_{chm} that is incremented by δt at each successful integration, until it reaches the value of the global time step Δt. Since a flame (reaction zone) can have a very complex shape, the computational load can have large fluctuations between different cells. If one attempts to vectorize along a row or a column, one may be forced to reiterate on the entire row only because a few cells are chemically active. To avoid this inefficiency and still be able to vectorize using long vectors (an obvious solution would be to vectorize with respect to the number of species N_s or the number of reactions N_{rea}, which are short vectors), we have devised a redistribution scheme. The method is to construct a "stack," or long vector, with the concentration data of all cells that are active. To construct this stack, we sweep along rows and columns and check the local time counter $t_{\text{chm}}(i,j)$; if $t_{\text{chm}} < \Delta t$, the cell is added to the stack. The chemical kinetics algorithm then operates on this stack, such that the inner loop runs along the stack index ($k = 1, \ldots, 256$ or more), and the procedure is repeated until all cells have reached the global time counter. The only scalar loop in the algorithm is, of course, the stack filling process, and is a negligible fraction of the overall computational cost.

The only major improvements in computational speed are obtained by reductions in the numbers of species and reactions, since the number of operations involved approximately scales as $N_s \times N_R$. Another significant improvement in the convection algorithm, as well as the computation of thermochemical properties (temperature, transport coefficients), is also obtained by reducing the number of species; therefore, the use of chemistry models is encouraged. In a previous paper, we have used a detailed reaction set (44 reactions, 9 species including N_2) for the numerical simulation of two-dimensional detonations on a ramp, in a hydrogen-air mixture (N_2 inert). In this present calculation, we used the set of Moretti (7 species, 16 reactions).[25] Our code can also use the global model of Rogers-Chinitz (5 species, 4 reactions)[26] with the ϕ correction. However, in mixing-controlled combustion, large variations of the stoichiometric parameter ϕ can occur. Since the Rogers-Chinitz model is strictly valid for $0.2 \leq \phi \leq 2$, it may not be appropriate to use in this case. Moreover, the choice of the ignition temperature $T_{\text{ig}} \simeq 1000$ K implies that the time scales may be completely wrong when the temperature is not clearly below or above this cutoff value. We plan to study in more detail the difference between the two models in future calculations. The Arrhenius rates chosen here are given in Ref. 27.

V. Rescaling and Subcycling

As observed by Bussing and Murman,[28] an implicit coupling between the convection and chemical kinetics provides an effective rescaling of the chemical time scale τ_{chem} to the time step used, i.e., τ_{conv}. This procedure is time-inaccurate and is practical for a small number of species involved, due to the expensive matrix operations. We have used instead an explicit, operator-splitting coupling. We have also experimented with an artificial rescaling of the chemical time scale by the stiffness parameter (i.e., the Damköhler number $\tau_{\text{conv}}/\tau_{\text{chem}}$), and found little difference in the results when the combustion is rapid. This rescaling can be easily done when the chemical kinetics estimates the time scale by which the combustion proceeds (basically $\tau_i + \tau_r$); instead of integrating up to Δt, one integrates up to $\tau_i + \tau_r$, thereby effectively slowing the combustion and reducing the stiffness. If the combustion was indeed faster than the convection, we expect little difference (taking into account the variation in signal propagation, $c \sim \sqrt{T}$) with the time-accurate method. It only means that our resolution is poor, and we cannot resolve the flame structure, which depends on the balance of the rates of convection and chemical changes. Therefore, a rescaling of the chemical time scale, whether done by an implicit or an explicit method, is valid for steady-state cases and if no attempt is made to resolve the flame structure accurately.

Using the explicit rescaling we found, however, only a small gain in computational speed. Most of the computational work is done during the heat release period τ_r, and only a small fraction during equilibration, where the chemical time step can be larger. If one rescales the chemistry such that $\tau_r \simeq \tau_{\text{conv}}$, the same number of iterations is required for the heat-release phase, and there is little gain. Using large time steps and a fully implicit method for the chemistry during τ_r and reducing the number of iterations can be potentially advantageous. However, as mentioned previously, it is potentially inaccurate and is practical only for a small number of species.

The use of patched grids allows us to increase the convergence rate by using the appropriate time step for each grid. Each grid can also be temporarily frozen, concentrating the computational activity in regions of nonequilibrium. This results in very significant computational cost savings.

An additional gain can be obtained by a subcycling of the physical process. In most cases studied, the species diffusion process, for example, took place with a time scale that was large compared to other processes (i.e., $\tau_d \gg \tau_{\text{conv}}$). If an intermediate time scale can be found, one can "skip" the diffusion operator, until τ_{int} is reached. We then effectively replace a large number of calls to the diffusion operator, each bringing a change of order $\tau_{\text{conv}}/\tau_d$ by a smaller number, each of order τ_{int}/τ_d. Depending on the individual cost of the operator being "accumulated," substantial savings can also be obtained this way.

VI. Numerical Results

We applied the numerical schemes described previously to some qualitative numerical simulations of detonations and flames attached to a wedge. We did not attempt to resolve some flow features completely (flame structure or viscous layers) and did not compare the chosen set of chemical rates with a more detailed set. More rigorous simulations are presently being planned.

The proof of concept of an ODWE relies on the creation of a detonation supported by a wedge or ramp in a supersonic stream. An experiment is presently being designed[11] to add support to this concept. The present numerical simulations were inspired by this experimental design.

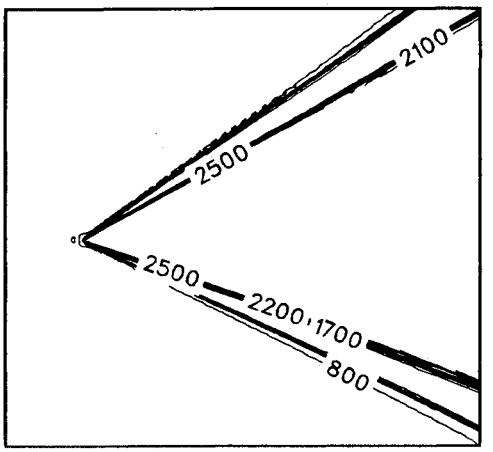

Fig. 1 Temperature for nonreacting stoichiometric case.

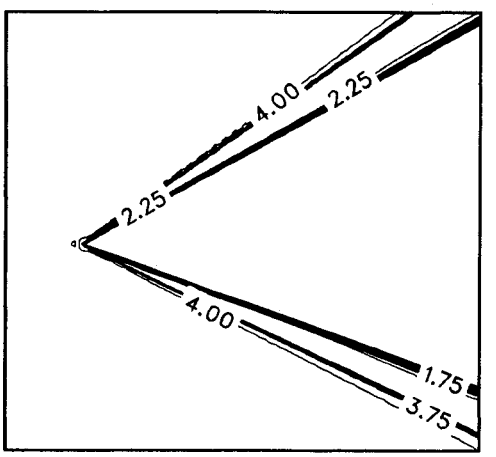

Fig. 2 Mach number for nonreacting stoichiometric case.

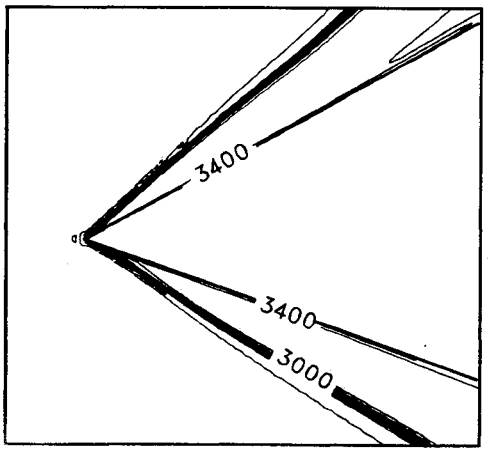

Fig. 3 Temperature for reacting stoichiometric case.

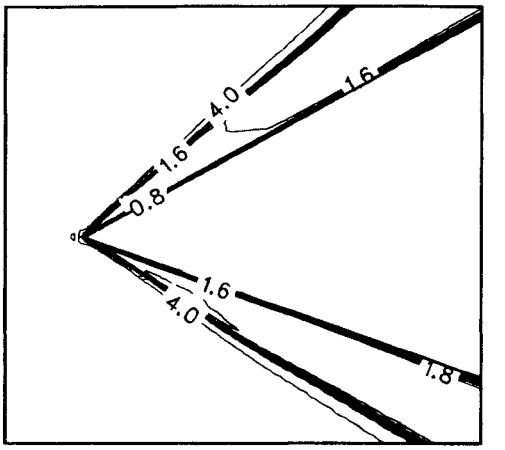

Fig. 4 Mach number for reacting stoichiometric case.

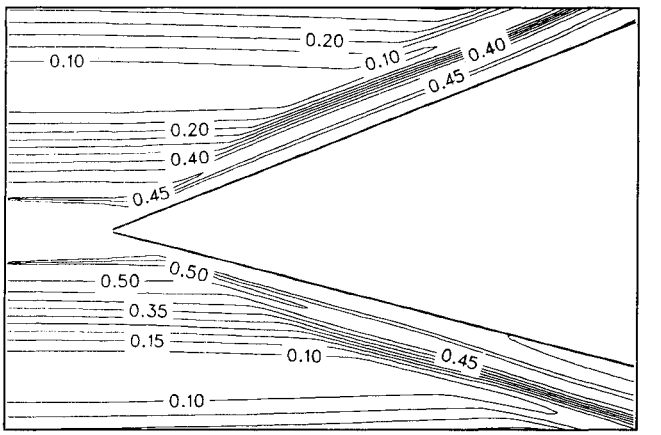

Fig. 5 H_2 concentration for nonreacting, variable ϕ case.

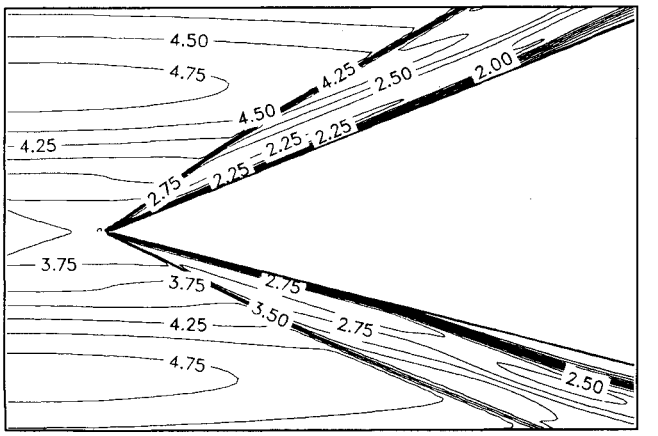

Fig. 6 Mach number for nonreacting, variable ϕ case.

Case A

As a first step, we create a detonation by placing a wedge into a supersonic stream of stoichiometric composition (hydrogen air). The wedge has an upper angle of 26.5 deg and a lower angle of 18 deg with respect to the stream direction. The length is $\Delta x = 5$ cm. The wedge surface is assumed adiabatic, and no-slip conditions are applied at the wall boundary.

Figures 1 and 2 show the temperature and Mach number profiles for the nonreacting case. This is not, however, an ideal-gas case, since the specific heats are allowed to vary with temperature. The temperature of the boundary layer is roughly 2200 K. The viscous sublayer is not resolved (the starting y^+

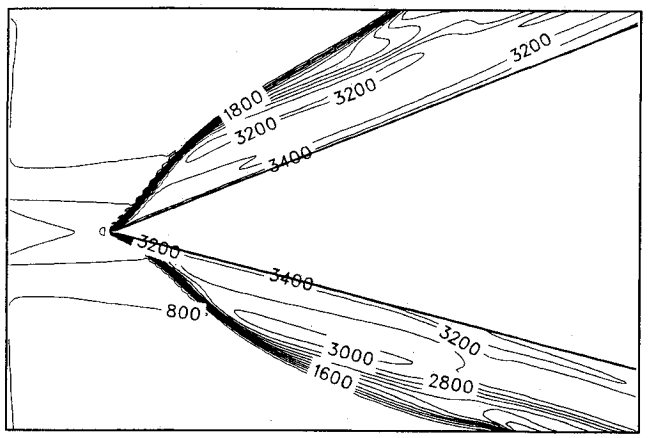

Fig. 7 Temperature for reacting, variable ϕ case.

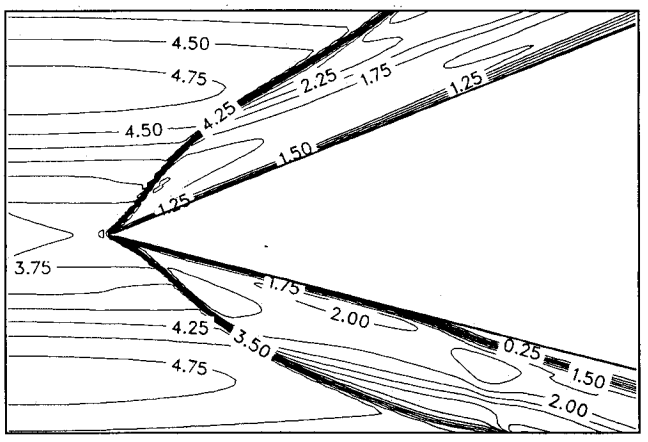

Fig. 8 Mach number for reacting, variable ϕ case.

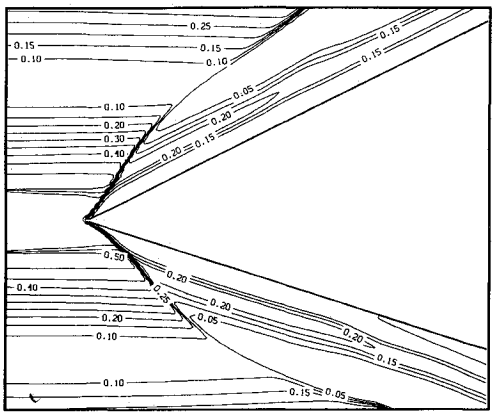

a) H_2 concentration for reacting, variable ϕ case

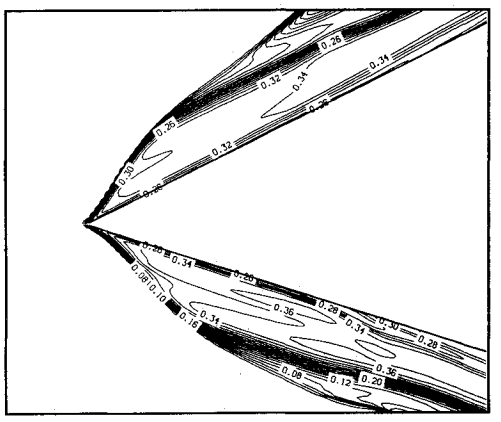

b) H_2O concentration for reacting, variable ϕ case

Fig. 9 Hydrogen and water concentration.

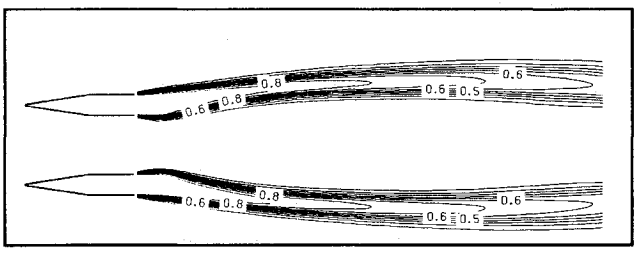

Fig. 10 H_2 concentration for fuel injection.

value is $\simeq 100$). Figures 3 and 4 show the profiles of the same quantities for the reacting case. The wave has steepened, as expected from simple analytical consideration.[3,12] The flow properties are uniform away from the boundary layer. The water concentration would show the same uniformity; the reaction zone is adjacent to the shock discontinuity.

Case B

More realistic configurations may involve considerable variations in mixing. To obtain some idea of the effect on the wave, we artificially modulated the freestream concentrations by a pseudosinusoidal function. The stoichiometric parameter ϕ is now allowed to vary from 0.1 to 1.9. The center region remains at $\phi = 1$. The freestream temperature is unchanged but the variations in molecular weight produce variations in Mach number. Additionally, the diffusion of species produces some variation of the temperature downstream of the left boundary.

Figures 5 and 6 show, respectively, the H_2 concentration profiles and Mach number profiles for the nonreacting case. There is a small modulation of the curvature of the wave front, due to the Mach number variation. The temperature of the boundary layer is almost unchanged from case A. To obtain a more accurate value at the wall, we need to increase the resolution further. However, our main interest does not at this point include such high accuracy for the boundary layer, and we therefore did not attempt a calculation with the necessary resolution.

Allowing for combustion, Figs. 7 and 8 show the temperature and Mach number profiles; the curvature fluctuations are now clearly enhanced. The combustion is nevertheless complete, i.e., all the hydrogen (or all the oxygen, the lesser of the two) is burned. The hydrogen and water concentration contours are shown in Figs. 9a and 9b. The recognition of a detonation wave becomes now more problematic, since the steepening of the wave is mixing-dependent. An interesting procedure would be to repeat the same experiment at different pressure. If the pressure is decreased, the chemistry time scales become larger, and the flame eventually decouples from the shock.

Case C

The logical extension to the previous simulations is to model a fuel injection process, then feed the flow to the wedge. We have experimented with several configurations of struts for the fuel injection. The first configuration consisted of three struts, of a generic shape separated by an equal distance, with fuel injection at the top and bottom of the flat parts. It was found, however, that the Mach number would drop too much ($M_\infty = 4$ to $M \simeq 1.5$) to be a practical method. It was suggested then to displace the center strut downstream, but this design proved to be no better. An interesting consequence of the shock structure

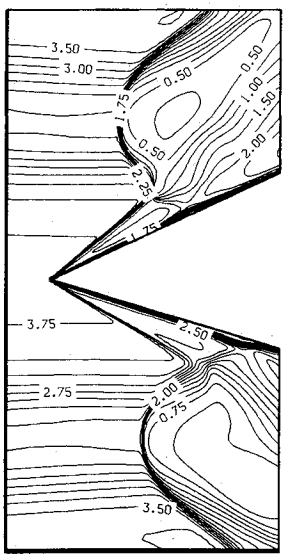

Fig. 11 Mach number, nonreacting case; input from strut flowfield.

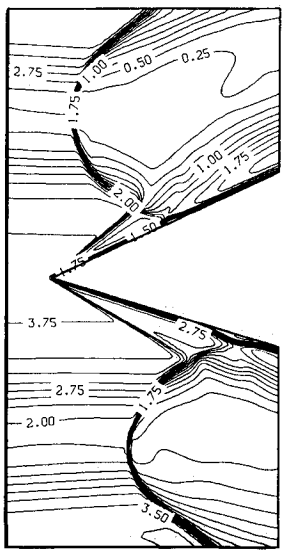

Fig. 12 H_2 concentration, nonreacting case; input from strut flowfield.

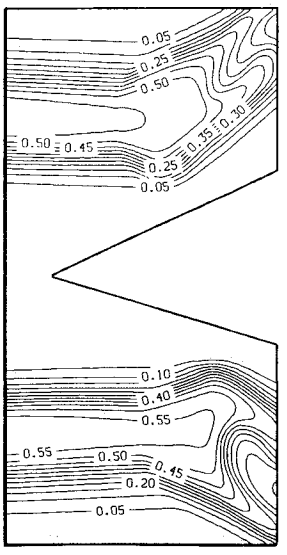

Fig. 13 Mach number, reacting case; input from strut flowfield.

in the fuel injection region was the presence of a large recirculation region in front of the injector, where fuel would accumulate. In addition, when injecting with high dynamic pressure for better penetration, the temperatures and pressure reached at the bow shocks lead to a rapid ignition of the fuel. We finally decided to model a two-strut configuration, where the fuel is injected from the base region. In addition, we modeled some active cooling of the strut surface by injecting cold (300 K) nitrogen gas at high pressure near the tip of the strut. Figure 10 shows the fuel concentration profiles obtained from this particular strut configuration. The fuel is accelerated to $M \simeq 3$ at the right boundary. (The white bands and the discontinuities of some of the profiles come from the patched grid boundaries.) With the help of the coolant injection, the temperature of the boundary layers and of the mixing layers is sufficiently low that no combustion occurs prematurely. We emphasize that we did not attempt to resolve completely the boundary layers and shear layers. To model the mixing in these regions accurately, one must resolve the length scales at exit plane of the fuel injection, since the initial instability produced there is responsible for the turbulent mixing. Such a simulation was beyond the scope of this work. Some other methods of fuel injection and their flowfields are presently being investigated.

The flowfield resulting from such a strut configuration is then fed as an input boundary condition to the same wedge used in the previous cases. The nonreacting case is shown in Fig. 11 for the Mach number. The strong curvature of the shocks is due to the large variations in Mach number of the flow. Figure 12 shows the H_2 concentration profiles; the curved shock acts as a diverging lens, spreading the fuel over a larger area. It is an interesting aspect of the shock properties, that could eventually be used to enhance the fuel penetration. After switching on the chemical reactions, we obtain the profiles shown in Figs. 13 and 14 for the Mach number and temperature. The hydrogen and water concentration profiles are shown in the plots of Figs. 15a and 15b. There is now little difference between the nonreacting and reacting cases, as far as the location of discontinuities is concerned. Most of the combustion takes place in two "tongues," where most of the mixing occurred. The combustion is fast, and the flame is coupled to the shock in that region, which is responsible for the slight upstream displacement of the wave front. More importantly, the detonation front is stable, despite the locally low values of the Mach number (estimated below M_{CJ}).

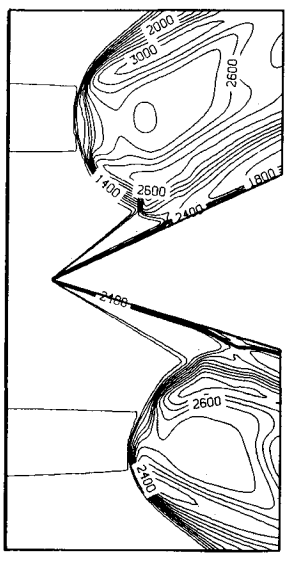

Fig. 14 Temperature, reacting case; input from strut flowfield.

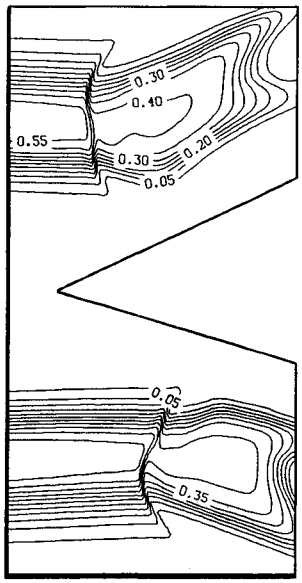

Fig. 15a H_2 concentration, reacting case; input from strut flowfield.

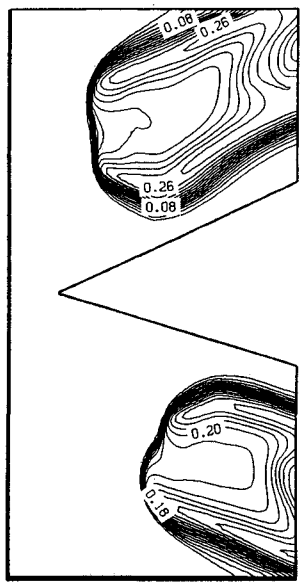

Fig. 15b H_2O concentration; input from strut flowfield.

VII. Conclusions

We have described a modern numerical capability that is still in a development process, and that is being tuned for the simulation of supersonic reacting flows. We have applied the code to the simulation of detonations and flames produced by a wedge inserted in a supersonic stream. "Pure" oblique detonations attached to the wedge have been produced in a stoichiometric, uniformly mixed hydrogen-air stream. The wave is seen to rotate upstream with the energy release, according to simple analytical arguments. By artificially spatially varying the mixing, stable curved detonation fronts were obtained; the combustion is always complete, and the flame is strongly coupled to the wave front. By using the results of a fuel injection pattern, we examined the detonation front in the poorest mixing conditions; the curvature is then dominated by the mixing properties (variation in molecular weight, Mach number) instead of the heat release fluctuations. Despite locally low Mach numbers, the detonation cannot propagate forward. This is expected from the analytical and computational models of detonation structure (absence of "detonation cells").[29] Therefore, in a realistic scramjet environment, the flames and detonations induced by a shock are mixing-controlled.

Although the design of an ODWE suffers from the impracticality of realizing an ideally mixed supersonic fuel-air stream, the concept can apparently be extended to the mixing-controlled environment. The use of a (curved) shock as a flame holder is still an appealing concept, especially at very high Mach numbers, whether the flame is attached to the shock or not. Another potential interest lies in the mixing enhancement that is expected to occur behind curved shock fronts.[30] It appears that the inhomogeneities in the mixing and Mach number variations from the fuel injection process are sufficient to create strong disturbances on the shock front, without additional help (acoustic or other). The effect of a shock train in a supersonic combustor is likely to be of major importance in its design.

The numerical capability is currently being enhanced: grid adapting and grid embedding is planned for the near future. A k-ϵ TVD code has also been recently designed and needs to be implemented and validated. Future calculations will also focus on further validation of the numerical methods, by direct comparisons with detonations and flames obtained in various mixtures.

References

[1]Roy, M., "Comptes rendus a l'Academie des Sciences," Paris, Feb. 1946.

[2]Townend, L. H., "An Analysis of Oblique and Normal Detonation Waves," Royal Aircraft Establishment, Farnborough, England, TR 3638, March 1966.

[3]Townend, L. H., "Detonation Ramjets for Hypersonic Aircraft," Royal Aircraft Establishment, Farnborough, England, TR 70218, Nov. 1970.

[4]Morrison, R. B., "Evaluation of the ODW Ramjet," NASA CR 145358, Jan. 1978.

[5]Sargent, W. M. and Gross, R. A., "A Detonation Wave Hypersonic Ramjet," Air Force Office of Scientific Research, TN 59-589, 1959.

[6]Burton Northam, G. and Anderson, G. Y., "Supersonic Combustion Ramjet Research at Langley," AIAA Paper 86-0159, Jan. 1986.

[7]Rhodes, R. P. et al., "The Effect of Heat-Release on the Flow Parameters in Shock-Induced Combustion," Arnold Engineering Development Center, TR-TN-TDR-62-78, May 1962.

[8]Gross, R. A., "Exploratory Studies of Combustion in Supersonic Flow, Parts I-IV," Project Squid, Contract NR-1858(25), NR-098-038, June 1959.

[9]Dugger, G. L., "Recent Advances in Ramjet Combustion," *ARS Journal,* Vol. 29, 1959, pp. 819-827.

[10]Nicholls, J. A. et al., "Stabilized Gaseous Detonation Waves," *ARS Journal,* Vol. 29, 1959, pp. 607-608.

[11]Adelman, H., Menees, G. P., and Balboni, J. A., "Analytical and Experimental Validation of the ODWE Concept," AIAA Paper 88-0097, Jan. 1988.

[12]Cambier, J. L., Adelman, H., and Menees, G. P., "Numerical Simulations of Oblique Detonations in Supersonic Combustion Chambers," *Journal of Propulsion and Power,* Vol. 5, Sept.-Oct. 1989, pp. 482-491.

[13]Harten, A., "High Resolution Schemes for Hyperbolic Conservation Laws," *Journal of Computational Physics,* Vol. 49, 1983, pp. 357-393.

[14]Yee, H. C., "Construction of Explicit and Implicit Symmetric TVD Schemes and Their Applications," *Journal of Computational Physics,* Vol. 68, 1987, p. 151.

[15]Yee, H. C. et al., "Implicit Total Variation Diminishing Schemes (TVD) for Steady-State Calculations," *Journal of Computational Physics,* Vol. 57, 1985, pp. 327-360.

[16]Yee, H. C. and Harten, A., "Implicit TVD Schemes for Hyperbolic Conservation Laws in Curvilinear Coordinates," AIAA Paper 85-1513, 1985.

[17]Yee, H. C., "Linearized Form of Implicit TVD Schemes for Multidimensional Euler and Navier-Stokes Equations," *Comp. & Maths. with Appls.,* Vol. 12A, 1986, pp. 413-432.

[18]Roe, P. L., "The Use of Riemann Problem in Finite Difference Schemes," *Proceedings of the 7th International Conference on Numerical Methods in Fluid Dynamics,* Lecture Notes in Physics, Vol. 141, Springer-Verlag, New York, 1981.

[19]Dixon-Lewis, G., *Combustion Chemistry,* edited by W. Gardner, Springer-Verlag, New York, 1984.

[20]Hirschfelder, J. O., Curtiss, C. F., and Bird, R. B., *Molecular Theory of Gases and Liquids,* Wiley, New York, 1954.

[21]Boris, J. P. and Jones, W. W., "An Algorithm for Multi-species Diffusion Fluxes," *Comp. Chem.,* Vol. 5, 1981, pp. 139–146.

[22]Smagorinsky, J., "General Circulation Experiments with Primitive Equations," *Journal of Fluid Mechanics,* Vol. 104, 1963, pp. 99–165.

[23]Rogallo, R. S. and Moin, P., "Numerical Simulation of Turbulent Flows," *Annual Review of Fluid Mechanics,* Vol. 16, 1984, pp. 99–137.

[24]Wang, J. C. T. and Widhopf, G. F., "A High-Resolution TVD Finite-Volume Scheme for the Euler Equations in Conservation Form," AIAA Paper 87-0538, Jan. 1987.

[25]Moretti, G., "A New Technique for the Numerical Analysis of Nonequilibrium Flows," *AIAA Journal,* Vol. 3, March 1965, pp. 223–229.

[26]Rogers, R. C. and Chinitz, "On the Use of a Global Hydrogen-Air Combustion Model in the Calculation of Turbulent Reacting Flow," AIAA Paper 82-0112, Jan. 1982.

[27]Ferri, A., "Mixing-Controlled Supersonic Combustion," *Annual Review of Fluid Mechanics,* Vol. 5, 1973, pp. 301–338.

[28]Bussing, T. R. A. and Murman, E. M., "A Finite-Volume Method for the Calculation of Compressible Chemically Reacting Flows," AIAA Paper 85-0331, 1985.

[29]Oran, E. and Boris, J. P., *Numerical Simulation of Reacting Flows,* Elsevier, Amsterdam, The Netherlands, 1987.

[30]Kumar, A. et al., "A Mixing Augmentation Technique for Hypervelocity Scramjets," AIAA Paper 87-1882, 1987.